Deuterium Retention and Morphological Modifications of the Surface in Five Grades of Tungsten after Deuterium Plasma Exposure

M. Balden, A. Manhard, S. Elgeti

Max-Planck-Institut für Plasmaphysik, Boltzmannstr. 2, D-85748 Garching, Germany

Abstract

Five tungsten (W) grades were simultaneously exposed to deuterium (D) plasma with 10^{20} D/(m^2s) of 38 eV/D up to 10^{26} D/m^2 at 500 K specimen temperature. The D inventories and their depth profiles within the topmost 12 µm were determined by nuclear reaction analysis (D(^{3}He,p)α). Morphological modifications at and below the surface were analysed by confocal laser scanning microscopy and scanning electron microscopy assisted by focused ion beam cross-sectioning. The observed variation of the D inventory by more than one order of magnitude (0.5-15x10^{20} D/m^2) is attributed only to the different properties of each W grade. Spherical blisters and stepped flat-topped extrusions are observed depending on the W grade. These modifications are interpreted as an indication for hydrogen loading-induced damaging. The exposure conditions and W grades were chosen to allow a comparison between published data sets.

Keywords: Tungsten, D retention, blistering, plasma-facing material

PACS numbers: 52.40.Hf, 61.72.Qq, 61.80.Jh

Corresponding Author:
Martin Balden

Postal Address:
Max-Planck-Institut für Plasmaphysik, Boltzmannstr.2, D-85748 Garching

Telephone: **+49 / 89 3299 1688**, Fax: **+49 / 89 3299 1212**

E-mail address: **Martin.Balden@ipp.mpg.de**

1. Introduction

Tungsten (W) is envisaged as plasma-facing material for future fusion devices [e.g. **1,2**]. In recent years many studies regarding the hydrogen retention and surface morphology were performed on various W grades [e.g. **3-20**]**.** The hydrogen retention varies by orders of magnitude depending on the ion beam and plasma exposure conditions (e.g., hydrogen flux, fluence, impact energy, temperature). Even if some dependences on exposure parameters were investigated in detail (e.g., on fluence and temperature), often the material and its final preparation vary from study to study. This variation can be expected to influence the retention [*19,***21,22**] and the surface morphology evolving during plasma exposure. Therefore, this variation hinders the comparability between different studies. It is still under discussion how the used W grades contribute to the observed variation in retention and to the observed morphological modifications of the surface, which range from about spherical blisters to stepped, flat-topped as well as volcano-like extrusions [e.g. *5,6,15,16*]. For assessing the retention and the erosion behaviour of tungsten grade used in future fusion devices, this question must be answered and a more basic understanding is necessary, also of the recrystallized material.

In this article, "**W grade**" is defined as the combination of the tungsten base material, its processing and the specimen preparation, which includes in particular polishing and heat treatments.

Two extensive studies of two groups ([*7-10*] and [*11-15*]) were performed with detailed parameter scans. The two groups investigated the deuterium retention with D depth profiling and the surface morphology evolution, each on well-prepared surfaces, but for different tungsten grades and different exposure conditions, in particular deuteron flux and fluence.

The first group [*7-10*] used as the typical exposure condition 38 eV/D, 6×10^{24} D/m^2, and 370 K at a flux of ~10^{20} D/(m^{2}s). They used a quantified plasma source [**23**] ("PlaQ") to expose rolled W material after four different heat treatments up to recrystallization. They performed fluence, energy and temperature scans around the condition given above, resulting in D inventories varying by more than three orders of magnitude up to nearly 10^{21} D/m^2. They also studied the blister size and areal density of the observed spherical blisters.

The second group [*11-15*] used W material from another manufacturer after polishing and after recrystallization. They determined the temperature dependence of the D inventory and the surface modifications at two higher fluences (10^{26} D/m^2 and 10^{27} D/m^2) also for 38 eV/D but with a hundred times higher flux (~10^{22} D/(m^{2}s)) at the Linear Plasma Generator ("LPG") at Japan Atomic Energy Agency, Tokai, Japan [**24**]. They detect D inventories up to slightly more than 10^{22} D/m^2 and a variation of D inventory with temperature between 300 and 800 K of more than three orders of magnitude. A variety of surface modifications – from large flat-topped (tens of µm) to volcano-like extrusions of different size (hundreds of nm up to several µm) – were observed and their sub-surface morphology was analysed.

The first aim of the present study is to allow a comparison between the two data sets briefly described above by using the same W grades as well as by choosing suitable exposure conditions at PlaQ, i.e., 10^{26} D/m^2 and 500 K. Therefore, only one main parameter varies to each published data set: fluence to [*7-10*] or flux to [*11-15*]. The second aim is to provide data belonging to a series of experiments dedicated to study

the influence of the ion flux during plasma exposure on surface morphology and deuterium retention. This joint action covers a flux range of about 4 orders of magnitude by using different exposure devices, from PlaQ with moderate flux of 10^{20} D/(m^2s) [*23*] via LPG with high flux of 10^{22} D/(m^2s) [*24*] to Pilot-PSI with very high flux of 10^{24} D/(m^2s) [**25**].

Therefore, in the study presented here, five different tungsten grades – including the ones predominantly studied in [*7-15*] – were exposed simultaneously to a D plasma in PlaQ, i.e., receiving the same exposure (specimen temperature: 500 K; D impact energy: 38 eV/D; flux: 10^{20} D/(m^2s); fluence: 10^{26} D/m^2). The fluence of 10^{26} D/m^2, which needed 12 days of continuous exposure at PlaQ, was chosen in order to allow the comparison with the higher flux experiments, e.g., with ~10^{24} D/(m^2s) at Pilot-PSI, DIFFER, Netherlands [*25*], where accumulating the same fluence takes only ~100 seconds.

2. Experimental Details

2.1. Specimens and preparation

Two tungsten base materials produced by two manufacturers (Plansee SE, Austria and A.L.M.T. Corp., Japan) were used for the five investigated specimens. The base material from Plansee has a guaranteed purity of 99.97 wt.%, while the Japanese material has a higher nominal purity of 99.99 wt.%. The Plansee material was delivered after two different deformation processes: rolling to a ~0.8 mm thick plate, or swaging to a rod of 40 mm diameter. The Japanese material has an unknown deformation history. Furthermore, two additional grades were produced by recrystallization of the material of both manufacturers. To distinguish these five specimens, they will be termed **WP-R, rc-WP-R, WP-S, WJ,** and **rc-WJ** throughout this paper (**P**=Plansee, **J**=Japan, **R**=rolled, **S**=swaged, **rc**=recrystallized).

The deformation process, e.g., hot- and cold-rolling, forging or swaging, leads to variations in the grain morphology (size and shape) and in preferred grain orientation, depending on the degree of deformation and specimen shape. In general, the grains are elongated along the rolling direction or the rod axis.

For the rolled tungsten from Plansee (**WP-R**) the (sub-)grain dimension perpendicular to the plate surface is the smallest with 0.5-1 µm, while parallel to the surface the typical size is 1-5 µm [**26, 27**] (see section 2.4). For this specimen type, the plate surface is the surface exposed to the plasma. The specimen size is 12x15 mm^2. In the swaged material from Plansee, the grains are elongated parallel to the rod axis with a length of 5-10 µm. Perpendicular to the rod axis the grains have typical sizes of 2-5 µm. As specimens, 15x12 mm^2 plates (~0.8 mm thickness) were cut with the 15x12 mm^2 surface perpendicular to the rod axis (**WP-S**). Therefore, the grains are elongated perpendicular to the specimen surface, which was later exposed to the plasma. Please note that this criterion – grains elongated perpendicular to the surface – is one requirement for W used in ITER [**28**] and is, therefore, frequently used in literature to quote such material as “ITER-grade” [e.g. *11,13,19*]. The specimens of the Plansee materials were polished as described in [*26*] to ensure removing all mechanical damage by residual grain deformation.

Specimens of 10x10x2 mm^3 were cut from the Japanese material with their 10x10 mm^2 planes perpendicular to the main deformation direction (**WJ**). This leads

also to elongated grains perpendicular to the specimen surface ("ITER-grade"). These specimens were polished by the Japanese manufacturers to a mirror finish (for quality of the polishing see [*11,13*]). The typical grain size parallel to the specimen surface is 1-3 µm, while perpendicular to the surface the size is 2-5 µm [*11*].

Two different treatments were applied to produce the two recrystallized specimens. The polished specimen of the rolled Plansee material was heated to 2000 K for 0.5 h in helium atmosphere in house (**rc-WP-R**). The polished specimen of the Japanese material was heated by the manufacturer to 2070 K for 1 h in hydrogen atmosphere (**rc-WJ**). The deformation processing of that specimen was different from that of the specimen **WJ.** The grain size parallel to the surface for the recrystallized specimens **rc-WP-R** and **rc-WJ** are 10-30 and 20-100 µm, respectively. The different size could be due to the differences in the degree of deformation, the impurity content and the recrystallization conditions.

The preferred orientation of the grains parallel to the exposed surface of the five specimens was determined by X-ray diffraction (XRD 3003 PTS diffractometer, Seifert/GE). The two faces of the specimens of the rolled Plansee material have different rolling texture, one dominated by (100) and (111) planes parallel to the surface and the other by (110) planes, i.e., still easily recognisable after recrystallization [*27*]. These textures are slightly altered by the recrystallization procedure [*27*]. For the specimen **rc-WP-R** the side dominated by (110) planes was exposed to the plasma, while for the specimen **WP-R** the side dominated by (100) planes. The swaged Plansee material has a <110> fibre texture. Therefore, the exposed surface of **WP-S** is dominated by (110) planes. The Japanese material shows also a type of rolling texture and the exposed specimen surface of **WJ** is also dominated by (110) planes. For the recrystallized specimen **rc-WJ**, no conclusive texture analysis was possible due to the large grain size and the statistical small number of analysed grains. An orientation analysis in the frame of another study on such recrystallized specimens [**29**] points to a soft texture with a higher amount of grains close to (110) and a lower amount of grains close to (111).

Before exposure, all specimens were heated at 1200 K for 1 h for degasing, stress relieving and removing of oxide layers.

Equivalent specimens to **WP-R, rc-WP-R, WJ,** and **rc-WJ** – same material and treatment – were studied in [*7-10,25,26*], [*7,8*], [*11,15*], and [*12-17*], respectively. All equivalent specimens of rolled Plansee material originate from a single sintering batch to ensure the same initial microstructure and chemical composition. Specimens cut from the same rod of swaged Plansee material as the specimen **WP-S** were investigated in [*18-20*]. Unfortunately, these specimens [*18-20*] were polished with a different procedure than the recipe described in [*26*].

2.2. Plasma exposure

The five specimens were implanted all at the same time with deuterium ions from a quantified plasma source at IPP Garching [*23*] named PlaQ, which delivers mostly D_3^+ ions (above 90% of ion flux). The implantation was performed at 500 K ± 10 K, and the chosen specimen bias (100 V) together with the plasma potential (~15 eV) led to a mean energy of 38 eV per deuteron for the dominant ion species D_3^+. The deuteron flux was nearly 10^{20} D/(m^2s). The specimens were continuously exposed for

12 days in order to accumulate a deuterium fluence of 10^{26} D/m^2. In [7-10,19,20] the same plasma device and the same conditions except fluence were used.

2.3. Deuterium retention analysis

To determine the total deuterium retention and the depth profile of D in W, ion beam analyses with the D(^{3}He,p)α nuclear reaction was used. The stepwise energy scan of the incident ^{3}He beam with the 3 MV tandem accelerator at IPP Garching allows to calculate the depth profile from data. The cross-section of this nuclear reaction peaks at ~620 keV ^{3}He energy [30]. The depth, which is probed for D, depends on the primary energy since the ^{3}He ions lose energy as they penetrate the target. The proton and α spectra measured at different ^{3}He energies were evaluated simultaneously to obtain the underlying depth profile by a sophisticated analysis program (NRADC) applying Bayesian statistics [31]. Eight energies of the incident ^{3}He from 0.5 to 6.0 MeV were used, which results in a maximum information depth of nearly 12 µm. (The depth resolution decreases with depth, e.g., at 5 µm it is ~1 µm [32]). The eight used ^{3}He energies were distributed on four measurement spots (A: 0.5 MeV, B: 0.69 MeV, C: 1.2 and 1.8 MeV, and D: 2.4, 3.2, 4.5, and 6.0 MeV). Each analysing spot had a size of 1 mm^2. The analyses were made about three months after the exposure and storage under vacuum. The D inventory results from the integration of the depth profile and is an average value over the area of the analysing spots. More details on the experimental set-up for the nuclear reaction analysis (NRA), the depth resolution and the data evaluation can be found in [7,8,29,31,32].

2.4. Surface morphology

The morphological modifications of the surface were investigated by confocal laser scanning microscopy (CLSM) and scanning electron microscopy (SEM). The height, the lateral dimensions and the lateral distribution of the modifications were determined by CLSM (LEXT OLS4000, Olympus). More detailed images of the surface were taken by SEM (HELIOS NanoLab 600, FEI and XL30 ESEM, FEI).

In order to analyse the morphological modifications of the topmost few micrometres below the surface, cross-sections were obtained by focused ion beam (FIB) cutting after coating the surface in situ with a Pt-C-layer. The FIB and the coating system are included in the HELIOS device. For SEM imaging, the normal of cross-section plane and electron beam include typically an angle of 38°.

The size and shape of the grains in the surfaces and in the cross-sections were analysed by SEM, which is sensitive to small variations in the grain orientation (crystal orientation contrast). That means the sub-grains separated by small-angle boundaries are detected and their size and shape is determined [27] (section 2.1).

Furthermore, the exposed surfaces were examined by energy dispersive X-ray spectroscopy (EDX). No obvious impurities were found.

2.5. D_2 gas content of cavities

For determining the gas pressure inside gas-filled cavities, a gas detection system installed at the vacuum chamber of the HELIOS device was used. This gas detection

system consists of a quadrupole mass spectrometer (QMS) and calibrated deuterium leak bottles with different gas flows (7.6×10^{-9} and 7.9×10^{-7} m^3Pa/s). The QMS was calibrated against the leaks before and after each measurement series. During the alternating sequence of stepwise hole-drilling into the blister by FIB and imaging by SEM, the D_2 gas puff resulting from opening the blister cavity was detected and quantified by QMS. In the sequence of SEM images, the elastic relaxation due to the pressure release could be observed and correlated to the D_2 gas puff (see [*10,* **33**]). Assuming that the cavity volume was equal to the volume of the feature above the surface (obtained from 3D-surface data by CLSM), the pressure was calculated using the ideal gas equation at 300 K. The uncertainty of the resulting pressure is estimated to be below 50%. The gas content was determined about 9 months after the exposure and storage under vacuum (interrupted by analyses).

3. Results and discussion

3.1. Deuterium inventory

Figure **1** shows the D inventory (bars) and the depth profiles obtained by NRA of the five specimens investigated here. This NRA D inventory is obtained by summing up the deuterium over the full range analysed by NRA of nearly 12 µm, which is the maximum depth accessible by the ^{3}He beam with the highest used energy of 6.0 MeV. For comparison, some literature data [*7,11,12,19,25,***34**] for the same W grades but slightly different exposure conditions are also included in Fig. **1(a)**. The details of these data are listed in Tab. **1**. For most of the published D inventories, except [*7*], the range analysed by NRA was only 7 µm (highest used ^{3}He energy: 4.0 MeV). Accordingly, the D inventory in our specimens within this range (7 µm) is also indicated in Fig. **1(a)** for better comparability with these literature values by the filled bars.

3.1.1 Considerations to D retention

Before discussing the data, some remarks should be made. The D inventory after D exposure represents the trapped deuterium. The solute D during the exposure is normally significantly smaller than the trapped inventory. Furthermore, if exposure takes place at elevated temperature, solute D in W is able to escape from the specimen after the exposure stops due to its high mobility [**35**]. The equilibrium concentration of the solute D at room temperature is below $<<10^{-6}$. The time needed to reach thermal equilibrium at room temperature could take several days for our specimens. Therefore, the depth profile of the deuterium concentration – normally determined at room temperature – is attributed to be a measure for the distribution of *occupied* traps.

It must also be considered that:

i) The D fluence and the exposure time are sufficient long that diffusing deuterium reaches all traps, at least within the depth analysed by NRA. This is valid for the 12 days exposure used here. We even may reach already steady-state permeation conditions. This situation is different for high flux exposures up to the same fluence.

ii) At elevated temperatures, the thermal energy overcomes the binding energy of some trap types, which leaves a certain fraction of the traps unoccupied. This is valid at 500 K as it could be concluded from the onset of deuterium desorption in

temperature programmed desorption (TPD) measurements [see, e.g. *7,11,17,19, 20,***36,37**]. (Note some of these traps can be occupied during cooling after exposure at elevated temperatures by the out-diffusing solute D.)

The nature of the traps is not exactly clarified, but it is often attributed to impurities, grain boundaries, vacancies, interstitials, dislocations, voids and pores [*36,37*,**38** and references therein]. A defect density could describe the latter five. Each W grade exhibits an intrinsic defect density, which is expected to be homogeneous with depth up to the surface, if the polishing is adequate [*26*]. If the polishing is not adequate, a layer with higher degree of defects is expected resulting in higher D concentration.

Furthermore, it must be considered that the plasma exposure itself induces defects, which may become visible as morphological modifications of the surface (see section 3.2). This dynamic defect production is expected to depend on impact energy, flux, fluence and, in particular, on temperature. It is proposed that the D oversaturation in the W lattice during the exposure, i.e., D concentration above the thermo-dynamical solubility limit, is responsible for this damaging [see e.g. *7,13,***39**]. These defects can be termed as *hydrogen loading-induced damage*. The resulting defect density is expected to vary with depth. Furthermore, it could be speculated that the defect density saturates with fluence up to a certain depth exceeding several micrometres.

In addition, in the implantation zone, which is only some nanometres, the oversaturation may overcome a threshold for further damaging resulting in higher defect densities. Unfortunately, the high observed D concentrations in the range of percent at the surface and in the topmost nanometres (resolution limit) cannot definitely be assigned to D trapped in the implantation zone but may also be due to D adsorption at the surface and to D bonded to carbon/oxygen contaminations.

The deuterium retained beyond the range analysed by NRA can be determined by TPD, where the complete volume of the specimen is degased, if sufficient high temperatures are applied, i.e., the *total D inventory* is detected. In the literature the ratio between the *total D inventory* determined by TPD to the *D inventory in the topmost 7 µm* for plasma exposure at 500 K reaches values up to 10 (e.g., ID no. 11 in Tab. **1**). This implies that the diffusion into the bulk and the occupation of the trapping sites beyond 7 µm dominate the total D retention. In the frame of this study TPD was not performed, but will be performed in our future studies focusing on the total D retention.

3.1.2 D retention and depth profiles

For the five specimens investigated here, the most striking result is that the D inventory determined by NRA varies by more than one order of magnitude between about 0.5-15x10^{20} D/m^2 (Fig. **1(a)**). Because all five specimens were exposed simultaneously, this variation is correlated only to the material properties and not to the exposure conditions. In this context, we consider the susceptibility to hydrogen loading-induced damaging also as a material property. This clearly shows that a simple comparison of literature data (e.g., [*7-10*] versus [*11-15*]) can be misleading, since a large part of the reported differences in D retention can already be explained by the different W grades.

The D depth profiles in Fig. **1(b)** show the typical spike at the surface, the “surface peak” (<0.03 µm [*7,8,11,12,19,20*]). The profiles are almost flat beyond this surface

peak up to the analysed range of ~12 µm. Published depth profiles of D in W for 500 K have the same qualitative shape [7,11,12]. Only the specimen **WP-S** shows a slight increase with depth. The D concentrations at depth beyond 1 µm vary by about two orders of magnitude for the five specimens.

It is remarkable that the D amount contained in the surface peak is about the same for all five specimens (~3x10^{19} D/m^2). This amount is only a minor fraction of the deuterium observed with NRA, except for the specimen **rc-WP-R**. For the specimen **rc-WP-R** the amount in the surface peak is about 60% of all D detected by NRA. (The surface peak of all specimens may contain contributions of adsorbed D on the surface, of implanted D, and D bonded to impurities.)

As the observed D depth profiles are flat over the depth analysed by NRA, except from the surface peak, it could be concluded that i) all defects acting as traps are occupied according to their binding energy and that ii) the hydrogen loading-induced damage is either homogeneously distributed over a depth of at least 12 µm or does not increase the defect density significantly above the intrinsic level. Unfortunately, information about the intrinsic defect density is only available for **WP-R** and **rc-WP-R** [7,27]. It is expected that less intrinsic traps exist in recrystallized tungsten than in strongly deformed material. This is valid for both materials separately, i.e., the D concentration is about an about one order of magnitude lower for the recrystallized specimens compared to the unrecrystallized ones. However, we observed surprisingly here that the specimen from the rolled Plansee material has a lower D concentration compared to the specimen of the recrystallized Japanese material. The reason for that is unclear. We speculate that the intrinsic impurities – even if they are nominally lower for the Japanese material – play the dominant rule defining the occupied trap concentration, i.e. the impurity distribution in the material and its chemical composition result in a defect concentration, which is higher for the Japanese material.

3.1.3 Comparison to literature data

From a detailed comparison of our *D inventories obtained by NRA* with the literature data using the same W grade at temperature close around 500 K (sensitive parameter), some statements about the fluence dependence of the D inventory in the topmost micrometres and about flux effects for each W grade can be made:

i) For specimens of the same grades as **WP-R** and **rc-WP-R**, applying only a 20th of the fluence (6x10^{24} D/m^2) with the same moderate ion flux [7] does not lead to a significantly lower D inventory at 500 K (ID no. 6 and 7). This points to saturation of the trapped D with fluence within the topmost micrometres already at 6x10^{24} D/m^2 at 500 K. Such saturation with fluence of D inventory within this region was already reported for these W grades at 370 K [7]. The saturation is even more obvious by directly comparing the D concentrations in the depth profiles at both fluences for each grade: They are about the same [7]. (E.g., in the depth of 1 to 8 µm the D concentration is about constant at 10^{-4} and ~2x10^{-5} for **WP-R** and **rc-WP-R**, respectively.)

The D concentration probably does not saturate if a much higher flux (~10^4 times) is applied to specimens of the same grade as **WP-R**. This is indicated by the two data points ID no. 8 and 9 [25]. For these two data points, their fluence varies by a factor of 10, which leads to a variation of the D retention of nearly a factor of two.

Furthermore, this exposure to a fluence of 10^{26} D/m^2 at much higher flux leads to a 3 times higher D inventory in the topmost 7 µm compared to the exposure with the moderate flux used in this study (Tab. **1**, compare ID no. 2 and 8). It could be concluded that more damage by oversaturation is introduced due to the higher flux [*39*].

ii) For specimens of the same grade as **WJ**, the obtained D inventory is about the same even if a 100 times higher flux was used to load the specimen up to the same fluence of 10^{26} D/m^2 [*11*]. This points to saturation of the D inventory at a fluence of 10^{26} D/m^2 independent of flux for that W grade. Furthermore, the published data for different fluences (10^{26} and 10^{27} D/m^2) point to saturation of the D inventory with fluence within the topmost micrometres (ID no. 10 and 11), while the total D inventory in the specimen determined by TPD still increases [*11*].

iii) For specimens of the same grade as **rc-WJ**, the 100 times higher flux used in [*12*] (ID no. 13) than the moderate flux used in the study here shows an increase in the D inventory in the topmost 7 µm by a factor of about 6 for a fluence of 10^{26} D/m^2. The D inventory at intermediate flux (ID no. 18) falls in between the D inventory of higher and moderate flux [*34*]. This indicates a flux effect.

Overall, higher fluxes seem to increase the defect density at least in the topmost micrometre (<7 µm), as it is indicated by the higher D inventories and more severe morphological changes (see section 3.2). Furthermore, the saturation of the D inventory with fluence within the topmost micrometres could be interpreted that all traps, which can be populated at 500 K, are filled and that no further defects acting as traps are created by further exposure, i.e., hydrogen loading-induced damaging saturates. Apart from that, diffusion of D into the bulk of the specimens beyond the topmost micrometres is expected to increase the *total D inventory* until steady-state permeation condition is reached.

3.2. Surface and sub-surface morphological modifications

Three different surface morphologies with lateral dimensions larger than 100 nm after the D exposure are observed on the five specimens studied here: i) no obvious effect of the D exposure on the surface morphology, ii) stepped flat-topped extrusions with partly round and partly edged circumference, which are mostly restricted to one grain, and iii) spherical blisters, which extend across many grains. In addition to these surface morphologies above 100 nm lateral dimension, structures with tens of nanometre lateral size are observed on all grades.

3.2.1 No micrometre-sized modifications

The two specimens with grains elongated perpendicular to the surface (**WP-S** and **WJ**; from both manufactures), do not show any obvious modification of the surface morphology with lateral dimensions larger than 100 nm after the D exposure. The surface morphology is dominated by the height differences between neighbouring grains due to the polishing procedure, which is of the order of 100 nm for **WP-S** and ~10 nm for **WJ**. Also in the sub-surface, i.e., the topmost micrometre below the surface (up to about 30 µm), no modifications were found, especially, no cavities or additional distorted areas (beside the existing distortions after polishing [*13*]). These two specimens, on the other hand, show the largest D retention. We therefore

conclude that these specimens contain already a high concentration of intrinsic traps. Since these traps already capture most of the implanted D and slowing down the penetration of the diffusion front into the bulk, it is possible that the high trap concentration suppresses the precipitation of D_2 in blisters by changing the stress situation in the material. On the other hand, the special microstructure of these samples possibly does not provide as many nucleation points for blisters and does not support the growth of the crack system along the grain boundaries as for, e.g. **WP-R** (see below). At 100 times higher flux, some blister-like features were observed on **WJ** [*13*] but only in the layer, which contains distortions due to the polishing. We therefore suspect that the absence of blisters on **WP-S** and **WJ** under the high fluence, moderate flux conditions investigated here is due to a combination of high intrinsic trap concentration and microstructure.

3.2.2 Stepped, flat-topped extrusions

The two recrystallized specimens, **rc-WP-R** and **rc-WJ**, show only stepped, flat-topped extrusions, but the areal density of the extrusions varies by more than one order of magnitude between these two specimens (<3 and >30 extrusions/mm^2, respectively). The low density on **rc-WP-R** could be the reason why the extrusions were not observed at lower fluences on the same W grade in [*7*]. Furthermore, in particular the extrusions on **rc-WP-R** tend to appear in clusters and are distributed quite inhomogeneously. In Fig. **2** examples of such flat-topped extrusions and their correlated sub-surface features for both recrystallized specimens are shown. The extrusions on **rc-WJ** have typical lateral sizes of 10-50 µm with heights of 0.1-1 µm (Fig. **2(b-d)**). On **rc-WP-R** their lateral sizes seem to be in average smaller (5-20 µm; Fig. **2(g)**), although it is difficult to derive statistically meaningful values due to the small number of extrusions. Nevertheless, this smaller extrusion size on **rc-WP-R** is possibly correlated to the smaller grain size.

Surface features of even smaller lateral size (around 1 µm), which were observed as volcano-like extrusions at higher flux (same temperature and same fluence) in [*12-15*], are missing on both recrystallized specimens. Already in [*13*], it is supposed that these volcano-like extrusions are related to the higher flux. They appear for fluxes between 10^{21} and 10^{22} D/(m^{2}s). This fits to our conclusion that higher fluxes produce more hydrogen loading-induced damage.

On both recrystallized specimens, the sub-surface features, i.e., cavities and crack systems, are always located at grain boundaries (Fig. **2(e,f,g)** [*15*]). Sometimes pairs of extrusions on two neighbouring grains separated by the grain boundary are observed. The corresponding cavity is located on the grain boundary, which is in these cases roughly perpendicular to the surface (Fig. **2(d,f)**). On the other hand, for extrusions extending over a few grains across grain boundaries, the respective cavities and crack systems follow grain boundaries roughly parallel to the surface (Fig. **2(c,e)**). For the large extrusion covering nearly a complete grain as shown in Fig. **2(c)**, the crack system is extended and points partly towards the surface (left white arrow in Fig. **2(e)**). It could be speculated that this grain is nearly de-bonded and may eventually get lost for even higher fluences. Compared with similar flat-topped extrusions reported in [*15*], which are explained by gliding along {110}⟨111⟩, the extrusions here have much more steps (e.g. Fig. **2(b)**), which are only a few tens of nanometres high. Probably, each gliding event is smaller generating only a step

height of tens of nanometres, but due to the longer exposure time much more gliding events may occur resulting in a larger number of steps.

It should be stressed that cracking inside a grain is not found for the specimens investigated here. Such cracking was, however, observed for higher fluxes [*12-15*] correlated to the volcano-like extrusions indicating a flux effect. Distortions inside the grains due to the D exposure are less pronounced for the moderate flux exposure than for the higher flux exposure [*12-15*]. Nevertheless, they exist as it is visible, e.g., in Fig. **2(h)** (black arrows) between the cavity and along its related extrusion up to the surface.

3.2.3 Spherical blisters

Figure **3(a,b)** shows typical about spherical blisters on **WP-R**. The blister size of this specimen varies from <5 up to 400 µm with a bimodal distribution. The two maxima of this bimodal distribution are around 300 µm and below 50 µm. The areal density for the larger (>100 µm) and the smaller ones are 0.3 and 0.5 blisters/mm^2, respectively. For blisters in the size range of 100-400 µm their height is 0.3-10 µm, while for smaller ones (<50 µm) it is below 1 µm. The blisters appear often in groups (Fig. **3(a)**), and frequently smaller blisters are on top of the huge ones. The corresponding cavity for the large ones is found in depths of around 10 µm, but individual cavities were observed even deeper than 20 µm. For the smaller ones with a size around 10 µm, the cavities and the crack system are found at a depth of about 1 µm. Furthermore, for several of the huge blisters, it is proven that they were filled with D_2 gas and the amount of gas was measured quantitatively. This resulted in a D_2 content of several 10^{13} molecules, which corresponds to a pressure of several ten MPa at 300 K (Fig. **3(c)**). This is consistent with earlier measurements on smaller blisters [*10, 33*].

It is remarkable that the single blister shown in Fig. **3(c)** contains about 0.4% of the D inventory calculated from the NRA result for the entire exposed surface (180 mm^2). Since around 50 blisters of comparable size exist on this specimen, the total amount of D_2 in these blisters might even come up to 20% of the inventory detected by NRA. However, we assume that this D_2 gas does not contribute to the NRA depth profile shown in Fig. **1(b)** because the blisters are too sparsely distributed and their cavity is too deep.

For lower fluences [*7*], the blisters density is shown to depend strongly on temperature and is determined to be 3 blister/mm^2 at 500 K with an average size below 50 µm for a fluence of $6\text{x}10^{24}$ D/m^{2}s. We determine a larger average size (100 µm), while the areal blister density is lower (<1 blisters/mm^2). The possible explanation of growth and merging of the blisters can be ruled out, because the depth of the crack system is not going up and down across the blister. Analysing the crack system of larger blisters by cross-sectioning, see e.g. Fig. **3(e)**, shows that its depth increases continuously from the border of the blister to the centre to the large maximal depth. Therefore, we favour that in our experiments the absolute temperature was slightly higher than in [*7*].

As shown by first results on specimens of the same grade as **WP-R** exposed to very high ion flux ($3\text{x}10^{24}$ D/(m^{2}s)) at Pilot-PSI [*25, 39*] for fluences of 10^{26} D/m^2 and 10^{27} D/m^2, the blister size is strongly reduced due to the higher deuteron flux. They have only a size of 1-5 µm while the blister density is increased to 10^4 blisters/mm^2.

This size and density of blisters is observed at the moderate deuteron flux used here for a fluence of $6x10^{24}$ D/m^2 at about 350 K [*7*]. Furthermore, due to the very high flux at Pilot-PSI smaller tiny extrusions with cracks and distortions below (lateral size of ~250 nm) occur [*25, 39*] as well as surface structuring on the nanometre scale (tens of nm) [*3,***40,41**]. These surface modifications, especially the extrusions, point to further damaging at higher deuteron fluxes. This damaging does not appear at our exposure conditions. A local overheating due to distorted thermal flow above cavities of the observed dimensions (micrometers) is negligible, even for these high heat flux conditions (~6 MW/m^2).

3.2.4 Nanometre-sized structures

Figure **4** shows exemplarily for two of the five specimens the structures present after exposure with tens of nanometre lateral size. The structures vary from ridges, over waves to dot-like structures. The variation is larger from grain to grain than between the specimens. No distinct difference exists between the different specimens. The correlation of these structures with grain orientation is obvious. Xu et al. [*40,41*] reported about similar structures on tungsten exposed to D plasma with very high deuteron flux. They determined the correlation between appearance and specific grain orientation. They found a flux above $3x10^{23}$ D/(m^{2}s) is necessary to form their structure, which they allocate to the extreme exposure condition used, i.e., an higher oversaturation in the very near surface. Following this interpretation, we need another explanation for the appearance under our exposure conditions. It could be speculated that our nanometre-sized structures (Figure **4**) are due to sputtering of a very small fraction of impurity ions in the plasma.

4. Summary

Five specimens of different tungsten grades – defining “grade” as the combination of tungsten base material, processing and preparation – were simultaneously exposed to a D plasma. The observed variation of the D inventory in the topmost micrometres of the plasma exposed surface by more than one order of magnitude can exclusively be attributed to the different properties of the W grades. This demonstrates the importance of knowing the exact “state” of the investigated specimens. Without that, comparability between published data is limited. Therefore, the same grades as used in [*7-15*] were exposed under conditions that were chosen to allow a comparison between two extended published data sets. That means increasing the fluence to 10^{26} D/m^2, which was not achieved in a moderate deuteron flux device before (PlaQ, 10^{20} D/(m^{2}s)) for the same grades [*7-10*], and to use on the other hand the W grade which was extensively investigated at higher flux but with the same fluence and energy per deuteron (LPG, 10^{22} D/(m^{2}s)) [*11-15*]. Exposures at 500 K with 38 eV/D were performed and evaluated in both published data sets. Therefore, the presented data allow a comparison between these two devices with different fluxes, and thus allow reliable conclusions about flux-dependent processes.

We demonstrated that increasing the ion flux from ~10^{20} to ~10^{22} D/(m²s) not only increases the amount of trapped D but also changes the evolution of the surface morphology. The comparison of morphological modifications for different fluxes indicates the presence of more hydrogen loading-induced damaging processes at higher fluxes, e.g., the appearance of volcano-like extrusions with cracking and

distortions inside single grains [*11-15,25*] as well as the nanostructures on the surface [*3,40,41*]. Other hydrogen loading-induced features, namely the stepped flat-topped extrusions, can already be created at moderate flux, and their appearance exhibits a strong dependence on the W grade. We therefore conclude that the enhanced retention at high ion fluxes is due to the much more intense material modification that is reflected by the evolving surface morphologies. To fortify the conclusions reached here further, the database at higher flux for the grades used in this study should be enlarged (see [*25, 39*]).

We also found that in tungsten irradiated to high fluences under moderate ion flux conditions, blisters of considerable size (around 300 µm) and D_2 gas content of tens of MPa can be created at depths larger than 20 µm. Furthermore, in specimens with a relatively high intrinsic trap density and grains that are elongated perpendicular to the specimen surface (**WP-S** and **WJ**), blistering or other strong surface modifications are apparently suppressed. We attribute this to deuterium being captured by traps instead of precipitating, to changes in the stress state by filled traps, or to the lack of blister nucleation points in their microstructure. In addition, on all specimens nanometre-scaled features are observed (Fig. 4). Their appearance varies from grain to grain, i.e., depends on grain orientation.

As an outlook, due to the observed strong temperature dependence of the D inventory under high flux conditions [*11-13*] it would be of interest to perform the high fluence experiment with moderate flux presented here at different temperatures. We plan to repeat the exposure discussed in this article to improve the blister size statistics and to perform some further analyses, in particular TPD.

Overall, the database on the dependence of the hydrogen isotope retention on the tungsten grade does not allow suggesting a particular one for future use. The W grades fulfilling the specifications for W used in ITER [*28*] exhibit higher retention than others do, while they suffer less surface modifications. The temperature range, especially at high fluxes, should be extended for perspectives beyond ITER to higher temperature.

Acknowledgement

The authors would like to thank V.Kh. Alimov, K. Isobe and T. Yamanishi (JAEA) for providing some specimens, G. Matern for specimen preparation, K. Sugiyama, J. Dorner, M. Fußeder and B. Tyburska-Püschel for assistance in measuring the NRA data, and W. Jacob and V.Kh. Alimov for fruitful discussions.

This project has received funding from the Euratom research and training programme 2014-2018.

Tables:

Tab. 1: Deuterium inventory data obtained by NRA and TPD with their respective exposure conditions for the five used tungsten grades in this study and from literature. All NRA data represent the D inventory up to a depth of 7 µm (4.0 MeV).

ID no.	Specimen	T [K]	flux [10^{20} D/(m^2s)]	fluence [10^{26} D/m^2]	energy [eV]	D inventory by NRA [10^{20} D/m^2]	D inventory by TPD [10^{20} D/m^2]	source
1	rc-WP-R	500	1	1	38	0.41 (0.47*))	- -	this study
2	WP-R	500	1	1	38	0.73 (1.12*))	- -	this study
3	WP-S	500	1	1	38	1.88 (4.25*))	- -	this study
4	WJ	500	1	1	38	10.33 (16.09*))	- -	this study
5	rc-WJ	500	1	1	38	1.18 (1.92*))	- -	this study
	W grade equivalent to specimen							
6	rc-WP-R	500	1	0.06	38	0.25 (0.27*))	0.92	[7]
7	WP-R	500	1	0.06	38	0.55 (0.63*))	4.21	[7]
8	WP-R	530	1.4E+04	0.7	~40	2.50	- -	[25]
9	WP-R	515	1.2E+04	6	~40	4.50	- -	[25]
10	WJ	490	100	1	38	12.8	27.1	[11]
11	WJ	500	100	10	38	12.5	111	[11]
12	rc-WJ	500	100	1	38	- -	11.1	[12]
13	rc-WJ	505	100	1	38	8.1	22.8	[12]
14	rc-WJ	480	100	10	38	50.0	125	[12]
15	rc-WJ	535	100	10	38	9.3	- -	[12]
16	rc-WJ	515	100	10	38	- -	56.0	[12]
17	rc-WJ	490	125	1	96	6.7	- -	#)
18	rc-WJ	490	10	1	96	2.60	- -	#)

*) The numbers in brackets are D inventory by NRA for the analysed depth of nearly 12 µm for this study (6 MeV) and nearly 8 µm for data from [*7*] (4.5 MeV).

#) Two specimens of the W grade equivalent to **rc-WJ** were exposed to the D plasma at the LPG [*24*] in the frame of the publication [*13*] at two fluxes differing by slightly more than one order of magnitude (0.1 and 1.25x10^{22} D/(m^2s)). In order to reach 490 K at the lower flux, the specimen was biased leading to a D energy for the dominant ion species of 96 eV/D instead of the before used 38 eV/D [*11-15*]. A fluence of 10^{26} D/m^2 was accumulated. Beside the surface morphology, which is discussed in [*13*], the D retention was determined by NRA depth profiling of the topmost 7 µm using ^{3}He energies between 0.6 and 4.0 MeV at the IPP Garching.

Figures

Fig. 1 (single column): (a) D inventories of five W specimens obtained by NRA for depth up to 7 µm (filled bars) and 12 µm (open bars). For comparison published D inventories up to 7 µm depth (NRA) and total D inventories (TPD) for the same W grades are given as symbols. The numbers beside the symbols refer to the ID no. in Tab. **1**. Note that several TPD data given in Tab. **1** are higher than $2x10^{21}$ D/m^2 and TPD is often labelled as TDS. (b) The respective D depth profiles for the five specimens presented as bars in (a). Note that the D amount in the surface peak (<0.03 µm) is the same within the error bars for all five specimens and a correlation with bulk concentration does not exist.

Fig. 2 (double column): Stepped flat-topped extrusions of the two recrystallized specimens: (a) Overview surface image of **rc-WJ**; (b-d) individual extrusions; (e,f) cross-section view of the respective extrusions shown in (c,d) at the same magnification; (g) overview surface image of **rc-WP-R**; (h) cross-section view of the extrusion shown in (g). The white arrows mark the extrusion in the overview images and the cavity in the cross-sections, which partly reaches depth larger than 20 µm. The dotted lines indicate the position of the cross-sections. The black arrows in (e) and (h) point to distortions inside the grains. With the dashed ellipse, an extrusion of only ~25 nm height is highlighted, while the maximal heights of the others are 450 nm (b), 800 nm (c), 300 nm (d) and 600 nm (g). The three cross-sections (e,f,h) are tilted by 38° (distances in vertical direction are compressed by a factor of 0.79 in the images), while the other images are not tilted. The horizontal scale bar of (c,d) are also valid for (e,f).

Fig. 3 (double column): Spherical blisters on rolled tungsten: (a,b) Two examples of blisters on **WP-R** obtained by CLSM (intensity images; the roughness on the specimen gets visible due to the higher contrast mode used in (b)); (c) three dimensional plot of the blister shown in (b); (d) mass 4 spike due to puncturing the blister shown in (b,c) with FIB. The blister cavity has a volume of ~$5.6x10^4$ µm^3 and contains ~$3.8x10^{13}$ D_2 molecules. This corresponds to a pressure of ~20 MPa at 300 K. The thickness of the blister cap in the blister centre is around 20 µm, while it is thinner at the border of the blister. (e) SEM cross-section view of another large blister. The cross-section is horizontally tilted by 38° with respect to the viewing plane (vertical bar), while the surface (feature less white area) by 52°. The square hole is due to puncturing with FIB before cross-sectioning.

Fig. 4 (single column): Examples of nanostructured surfaces of (a) **WP-S** and (b) **WP-R** due to the plasma exposure (500 K, 38 eV/D, 10^{20} D/(m^{2}s), 10^{26} D/m^2). The variation of these structures between grains of different orientation is larger than between all W grades.

References

[1] Federici G et al 2003 J. Nucl. Mater. **313–316** 11

[2] Philipps V 2011 J. Nucl. Mater. **415** S2

[3] Tokunaga K et al 2005 J. Nucl. Mater. **337-339** 887–891

[4] Nishijima D et al 2005 Nucl. Fusion **45** 669

[5] Ueda Y 2004 Nucl. Fusion **44** 62

[6] Shimada T et al 2003 Fusion Engineering and Design **66-68** 247

[7] Manhard A 2010 *Deuterium Inventory in Tungsten after Plasma Exposure: A Microstructural Survey* (Ph.D. Thesis, University Augsburg), Technical Report IPP 17/34, Garching 2012.

[8] Manhard A et al 2011 J. Nucl. Mater **415**, S632

[9] Manhard A et al 2011 Phys. Scripta **T145** 014038

[10] Balden M et al 2011 J. Nucl. Mater. **414** 69.

[11] Alimov VKh et al 2012 J. Nucl. Mater **420** 519

[12] Alimov VKh et al 2011 J. Nucl. Mater. **417** 572

[13] Lindig S et al 2011 Phys. Scripta **T145** 014039

[14] Alimov VKh et al 2009 Phys. Scripta **T138** 014048

[15] Lindig S et al 2009 Phys. Scripta **T138** 014040

[16] Shu WM et al 2009 J. Nucl. Mater. **386–388** 356

[17] Shu WM et al 2007 Nucl. Fusion **47** 201

[18] Ogorodnikova O et al 2008 J. Appl. Phys. **103** 034902

[19] Ogorodnikova O et al 2009 Phys. Scripta **T138** 014053

[20] Ogorodnikova O et al 2011 Phys. Scripta **T145** 014034

[21] Luo G-N et al 2009 Nucl. Instr. Method B **267** 3041-45

[22] Wang P, Jacob W, Gao L, Elgeti S, Balden M 2014 Phys. Scripta **T159** 014046

[23] Manhard A et al 2011 Plasma Sources Sci. Technol. **20** 015010

[24] Luo G-N et al 2004 Rev. Sci. Instrum. **75** 4374

[25] ’t Hoen MHJ , Mayer M, Balden M, Lindig S, Manhard A, Kleyna AW, Zeijlmans van Emmichoven PA 2013: High Flux and Fluence Exposures of Pre-Irradiated Tungsten to Deuterium Plasmas, Proc. 14th Intern. Workshop on Plasma-Facing Materials and Components for Fusion Application, May 13–17, 2013, Jülich, Germany

[26] Manhard A et al 2013 Practical Metallography **50** 5-16

[27] Manhard A, Balden M, Elgeti S: Quantitative microstructure analysis of polycrystalline tungsten after different heat treatments, submitted to Materials Characterization

[28] ITER Material Assessment Report 2004, G 74 MA 10 01-07-11 W 0.2

[29] Voitsenya VS et al 2013 Nuclear Instruments and Methods in Physics Research B **302** 32-9

[30] Alimov VKh et al 2005 Nucl. Instr. Meth. B **234** 169-175

[31] Schmid K and von Toussaint U 2012 Nucl. Instr. Meth. B **281** 64-71

[32] Bielesch S, Oberkofler M, Becker H-W, Maier H, Rogalla D, Schwarz-Selinger T, Linsmeier C 2013 Nuclear Instruments and Methods in Physics Research B **317** 121-5

[33] Balden M, Lindig S, Manhard A, Alimov VKh, Ogorodnikova OV, Roth J 2011: Hydrogen gas filled cavities under surface extrusions on hydrogen-implanted tungsten, 13th International Workshop on Plasma-Facing Materials and Components for Fusion Applications and 1st International Conference on Fusion Energy Materials Science, May 9–13, 2011, Rosenheim, Germany, P51A

[34] Balden M, Lindig S, Alimov VKh, Manhard A, Tyburska-Püschel B unpublished data, see footnote of Tab. 1

[35] Causey RA and Venhaus TJ 2001 Physica Scipta **T94** 1-9

[36] vanVeen A et al 1988 J. Nucl. Mater. **155-157** 1113-7

[37] Eleveld H and van Veen A 1994 J. Nucl. Mater. **212-215** 1421-5

[38] ‘t Hoen MHJ et al. 2012 Nucl. Fusion **52** 023008

[39] ‘t Hoen MHJ M Balden M, Manhard A, Mayer M, Elgeti S, Kleyn AW and Zeijlmans van Emmichoven PA: Surface morphology of tungsten after exposure to high-flux deuterium plasmas, submitted to Nuclear Fusion

[40] Xu HY, Luo GN, Schut H, Yuan Y, Fu B.Q, Godfrey A, Liu W, De Temmerman G, 2014 J. Nucl. Mater. **447** 22-7

[41] Xu HY, Zhang BY, Yuan Y, Fu BQ, Godfrey A, De Temmerman G, Liu W, Huang H, 2013 J. Nucl. Mater. **443** 452-7

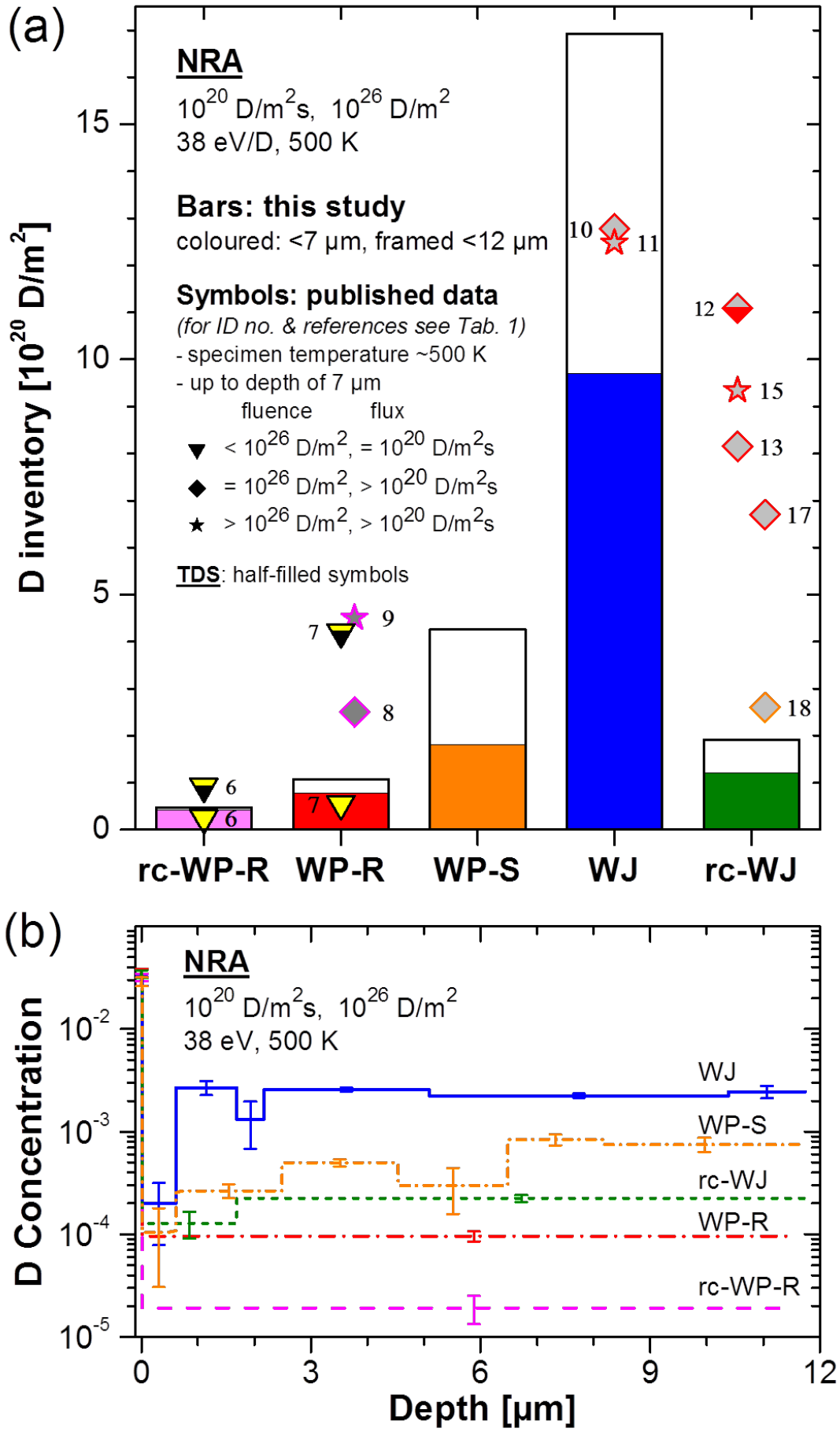
(a)
NRA
10^20 D/m^2s, 10^26 D/m^2
38 eV/D, 500 K
Bars: this study
coloured: <7 µm, framed <12 µm
Symbols: published data
(for ID no. & references see Tab. 1)
- specimen temperature ~500 K
- up to depth of 7 µm
fluence flux
< 10^26 D/m^2, = 10^20 D/m^2s
= 10^26 D/m^2, > 10^20 D/m^2s
> 10^26 D/m^2, > 10^20 D/m^2s
TDS: half-filled symbols
D inventory [10^20 D/m^2]
rc-WP-R
WP-R
WP-S
WJ
rc-WJ
(b)
NRA
10^20 D/m^2s, 10^26 D/m^2
38 eV, 500 K
D Concentration
Depth [µm]
WJ
WP-S
rc-WJ
WP-R
rc-WP-R

Fig1

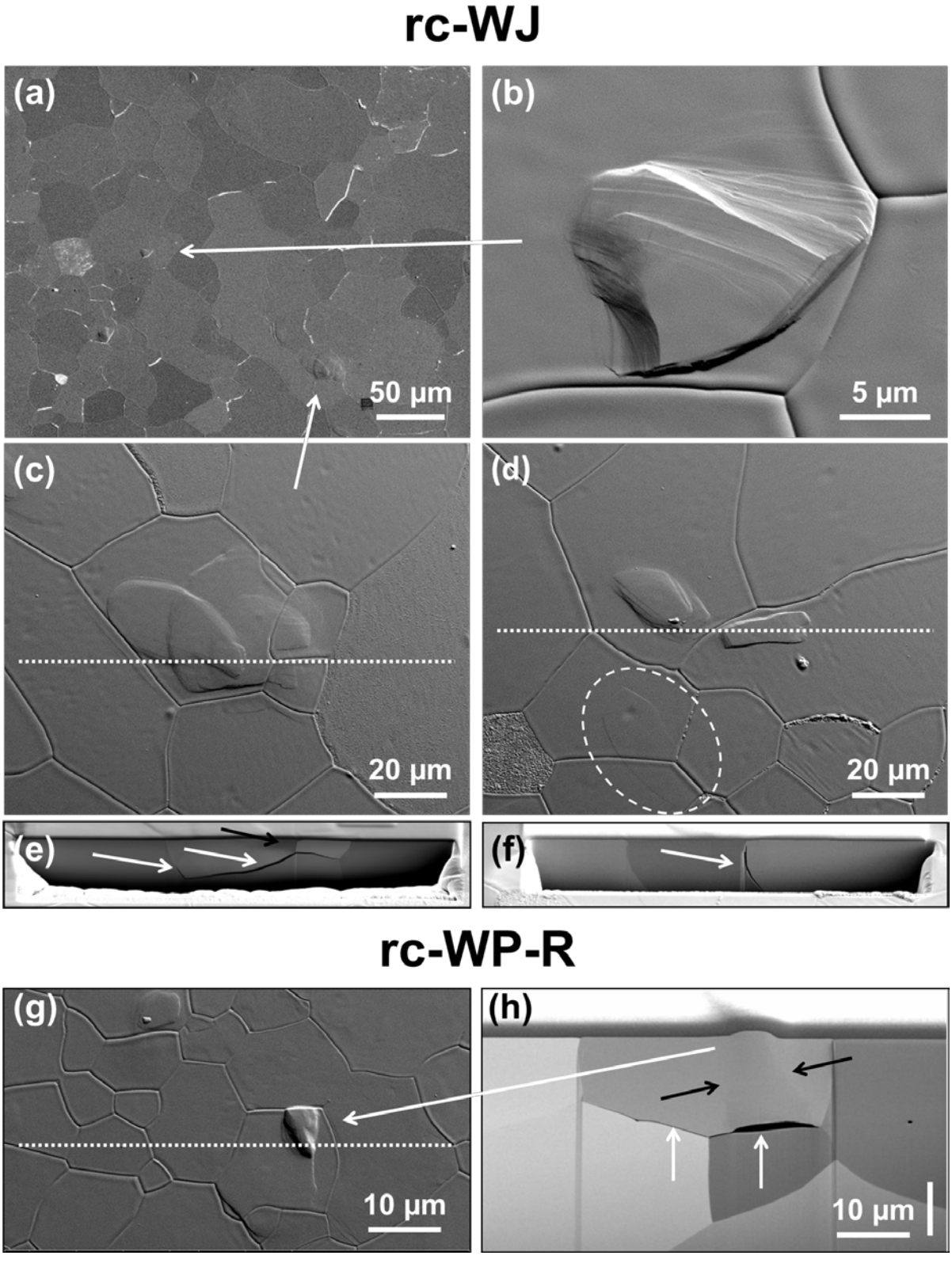

Fig.2

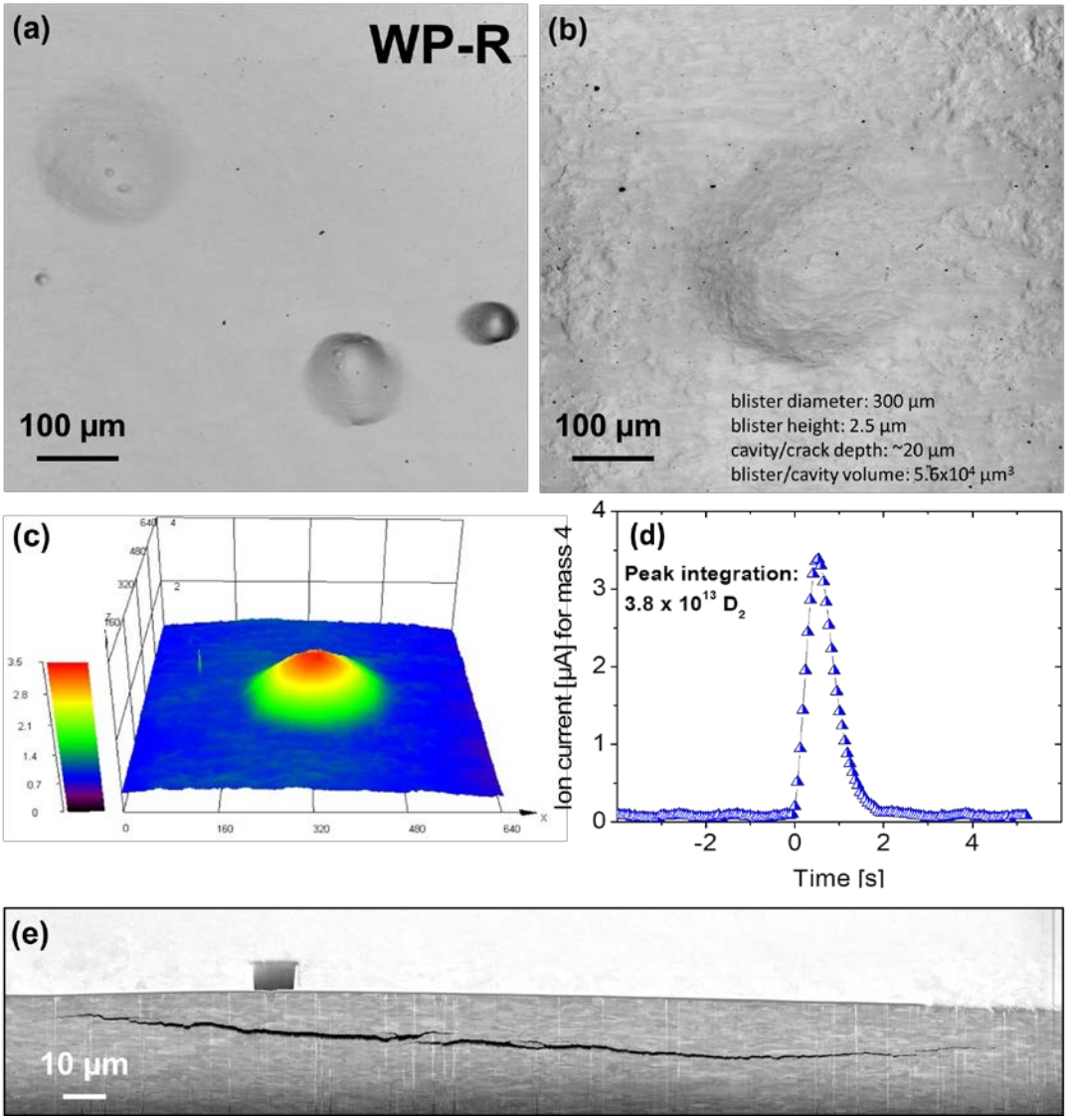
(a)
WP-R
100 µm
(b)
100 µm
blister diameter: 300 µm
blister height: 2.5 µm
cavity/crack depth: ~20 µm
blister/cavity volume: 5.6x10⁴ µm³
(c)
(d)
Peak integration:
3.8 x 10¹³ D₂
Ion current [µA] for mass 4
Time [s]
(e)
10 µm

Fig.3

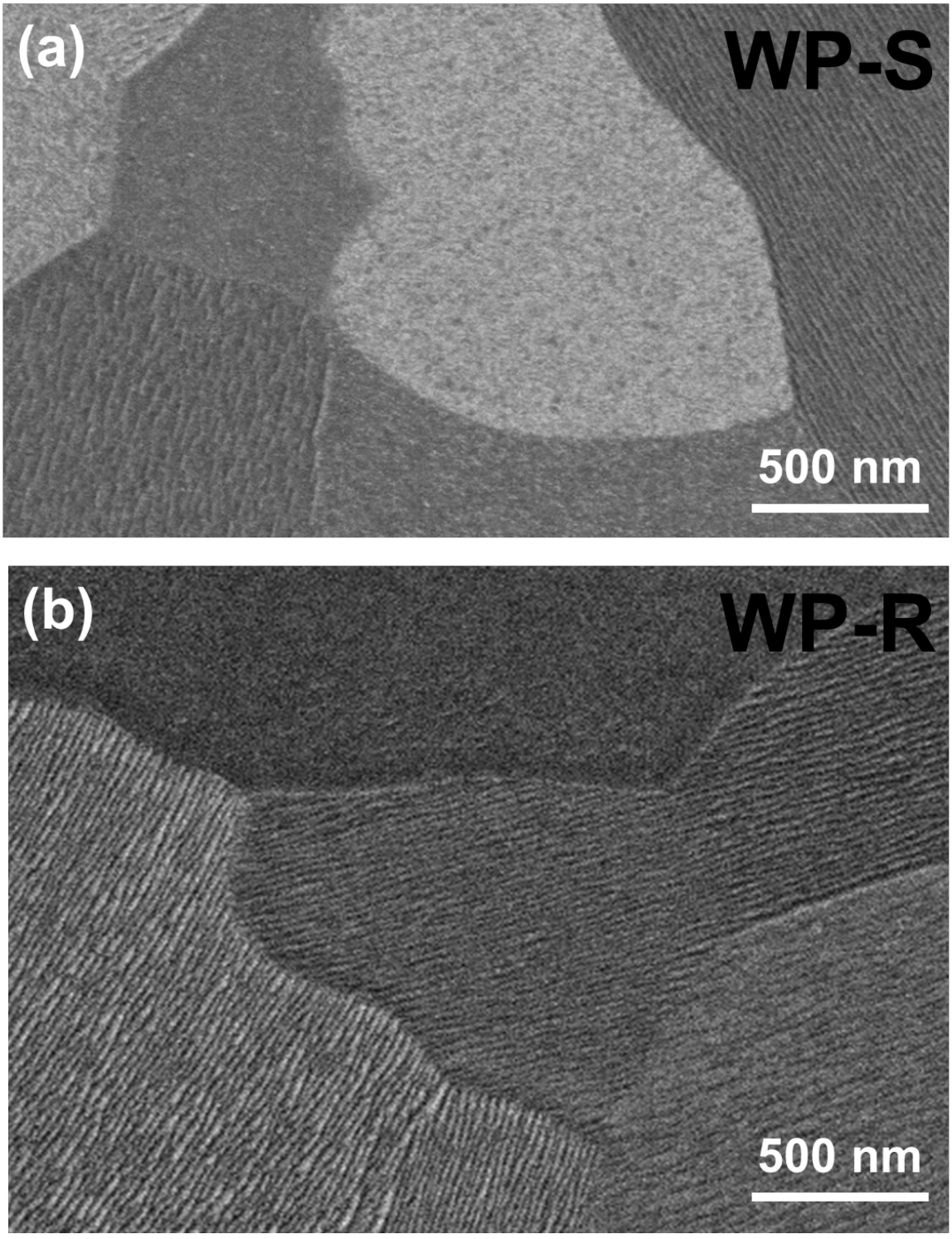

Fig. 4